Bulgarian Chemical Communications, Volume 49, Special Issue A (pp. 110–118) 2017

Crystallization of gels in the binary $TiO_2 – M_nO_m$ ($M_nO_m = TeO_2$, SeO_2, B_2O_3, ZnO) systems

A. Bachvarova-Nedelcheva[1]*, R. Iordanova[1], R. Gegova[1], Y. Dimitriev[2]

[1] *Institute of General and Inorganic Chemistry, Bulgarian Academy of Sciences, "Acad. G. Bonchev" str., bld. 11, 1113 Sofia, Bulgaria*
[2] *University of Chemical Technology and Metallurgy – Sofia, "Kl. Ohridski" blvd, 8, 1756 Sofia, Bulgaria*

Received October, 2016; Revised December, 2016

The present investigation deals with the sol-gel synthesis and phase characterization of binary $TiO_2 – M_nO_m$ ($M_nO_m = TeO_2$, SeO_2, B_2O_3, ZnO) powders with nominal composition $80TiO_2.20M_nO_m$. The competitive influence of different components on the phase formation was verified. According to XRD analysis the heat treated up to 300 °C gels exhibit a predominantly amorphous phase and formation of metallic tellurium or TiO_2 (anatase). The amount of amorphous phase gradually decreases with the temperature increase. Further increase of the temperature (700 °C) results in obtaining of polyphase products containing a mixture of several crystalline phasses (rutile, anatase, $TiTe_3O_8$ and $ZnTiO_3$). The heat treatment of the compositions containing H_2SeO_3 or H_3BO_3 leads to earlier crystallization of TiO_2 (anatase) about 300 °C while in the case of compositions containing Zn acetate or H_6TeO_6, TiO_2 is formed at higher temperatures 400 and 500 °C, respectively.

Keywords: sol-gel, composites, X-ray diffraction.

INTRODUCTION

The sol-gel method is an attractive alternative to the melt quenching route that may be used to extend synthesis and application of new compositions which are usually difficult to be prepared by conventional ceramic routes. Most of the problems that arose during the synthesis of these compositions are related to high melting temperatures, tendencies toward crystallization or liquid phase separation [1]. The sol-gel method also allows to overcome the problems with evaporation of some components such as SeO_2 [2]. It is well known that for the sol-gel synthesis, the titania (TiO_2) is widely used as a main component because its alkoxides are well developed. Up to now low temperature glasses are obtained in the TiO_2–TeO_2 binary system rich in TeO_2 (> 70 mol%) by melt quenching [3–5] and sol-gel techniques [6, 7]. First investigations in this system were performed by Weng and Hodgson which in a series of papers reported for the successful synthesis of TeO_2 based thin films and powders [6, 8–10]. Hayakawa et al. [7] prepared the TeO_2/TiO_2 thin films by sol–gel method and studied their optical properties. However, there are scarce data for the sol-gel synthesis of rich in titania (above 70 mol%) TiO_2/TeO_2 compositions [10]. For the binary TiO_2–SeO_2 system, several papers have been published concerning mainly the photocatalytic properties of obtained composites [11–16]. In the other binary TiO_2–B_2O_3 system, glasses have not been obtained and in the wide concentration range TiO_2 crystallize and phase separation was observed [17]. The photoactivity of TiO_2–B_2O_3 catalysts was improved by the boron content [18]. Up to now, many studies have described the sol-gel synthesis of composite materials in the binary TiO_2-ZnO system and their enhanced photocatalytic activity [19, 20]. It was found that the coupled semiconductor TiO_2/ZnO photocatalyst exhibits higher photodegradation efficiency compared to that of the single phase [21–23]. Among all investigations on metal or non – metal ion doping of TiO_2 there are still many unsolved problems concerning the competitive influence of the second component on the phase transformations of TiO_2 upon the heating as well as the thermal stability of the obtained products. This additionally motivates our study, which is a part of our investigations on sol–gel derived composite powders in dif-

* To whom all correspondence should be sent:
E-mail: albenadb@svr.igic.bas.bg

ferent binary and ternary systems [24–30]. Several oxides were selected as a second component: a classical network former (B_2O_3), conditional network formers (TeO_2, SeO_2) and an intermediate oxide (ZnO). Bearing in mind our experience on glass formation, structure and properties in different tellurite, selenite, titanate and borate systems as well as the problems that arose during their synthesis [1, 2, 31], we selected several samples with nominal composition $80TiO_2.20M_nO_m$ ($M_nO_m = TeO_2$, SeO_2, B_2O_3, ZnO) (Table 1).

The present investigation deals with the thermal stability of selected binary gels as well as their phase evolution upon heating up to 700 °C. The competitive influence of different components on the phase formation is verified.

EXPERIMENTAL

Samples preparation

Several samples with nominal compositions $80TiO_2.20M_nO_m$ ($M_nO_m = TeO_2$, SeO_2, B_2O_3, ZnO) have been selected for detailed investigation. They are situated in the gel formation regions pointed out in our previous investigations [24, 29, 32]. The gelation time for the investigated compositions was from 1 to 5 mins. The aging of gels was performed in air for several days in order to allow further hydrolysis. The compositions, for which precipitates were observed during the synthesis, were not considered as gels and they were not included in the gel formation regions. The investigated compositions are denoted as follow: $80TiO_2.20TeO_2$ (*sample A*), $80TiO_2.20SeO_2$ (*sample B*), $80TiO_2.20B_2O_3$ (*sample C*) and $80TiO_2.20ZnO$ (*sample D*). A different scheme for synthesis with new combination of precursors (organic and inorganic) was applied in this study. Titanium butoxide was used as a main precursor, while the other components were introduced as telluric (VI) acid (H_6TeO_6), selenous acid (H_2SeO_3), boric acid (H_3BO_3) and zinc acetate [$Zn(O_2CCH_3)_2.2H_2O$]. Zinc acetate was used instead of zinc nitrate because during the experiments gels were not obtained using the inorganic precursor. As it was already mentioned in our previous papers, the additional reason to use telluric (VI) acid instead of tellurium alkoxides is its high hydrolysis rate [33, 34]. Ethylene glycol ($C_2H_6O_2$) (99% Aldrich) was chosen as a main solvent. The scheme for synthesis is presented in Figure 1. Solutions (A and B) were prepared via dissolution of the precursors in ethylene glycol by means of vigorous stirring. Thus, transparent gels were obtained and their aging was performed in air for several days in order to allow further hydrolysis. The as-prepared gels were subjected to heating at ~150 °C and subsequently to calcination in the temperature range 200–700 °C. The stepwise heating of the samples from 200 to 700 °C for one hour exposure time in air was performed, until powders were obtained. The calcination temperature was selected on the basis of our previous investigations [24–30].

Samples characterization

The decomposition process of the as prepared and aged in air gels was determined by differential thermal analysis (LABSYS™ EVO apparatus) with Pt-Pt/Rh thermocouple at a heating rate of 10 K/min in air flow, using Al_2O_3 as a reference material. The accuracy of the temperature was ± 5 °C. The heating of the samples was limited up to 600 °C. Bearing in mind that the selenite materials are characterized with high volatilization tendency and the sublimation of SeO_2 occurs above 315 °C at atmospheric pressure the DTA – TG was not performed for sample B ($80TiO_2.20SeO_2$). Gases evolved (EGA) during the thermal treatments were analyzed by mass spectrometry (MS) with a Pfeiffer OmniStar™ mass spectrometer. Mass spectra recorded for samples A, C and D (Fig. 3a, b, c) show the m/z= 15, 18 and 44 signals, being ascribed to CH_3, H_2O and CO_2, respectively. Powder XRD patterns of the heat treated in the temperature range 200–700 °C powdered samples were registered at room temperature with a Bruker D8 Advance diffractometer using Cu-Kα radiation. The average crystallite sizes of the powders at selected temperatures were calculated using Sherrer's equation. The morphology of selected samples was examined by scanning electron microscopy (SEM) using a JEOL JSM 6390 electron microscope (Japan), equipped with an ultrahigh resolution scanning system (ASID-3D). The accelerating voltage was 20 kV, I ~65 μA. Transmission Electron Microscopy (TEM) investigations were performed on a JEOL JEM 2100 instrument at an accelerating voltage of 200 kV. The specimens were prepared by grinding and dispersing them in ethanol by ultrasonic treatment for 6 mins. The suspensions were dripped on standard carbon/Cu grids. The measurements of lattice-fringe spacing recorded in HR-TEM micrographs were made using digital image analysis of reciprocal space parameters. The analysis was carried out by the Digital Micrograph software.

RESULTS AND DISCUSSION

Thermal stability of the gels

The transparent gels were prepared applying the scheme shown in Figure 1 that summarizes all ex-

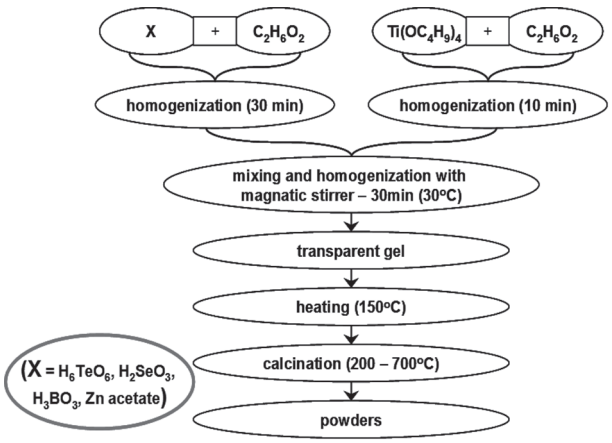

Fig. 1. Scheme for the sol-gel synthesis of TiO_2/M_nO_m gels.

perimental details already discussed above. The gelation proceeded immediately and the gel formation regions in the binary systems $TiO_2 – TeO_2$, $TiO_2 – SeO_2$, $TiO_2 – B_2O_3$ and $TiO_2 – ZnO$ were determined (Fig. 2a–d).

DTA/TG curves of as-prepared gels (samples A, C and D) are presented in Fig. 3a–c and their thermal stability was compared to those of pure Ti butoxide [32]. The thermal stability of pure Ti butoxide (TBT) was already discussed in our previous investigations [32]. Generally, several peaks are marked on the DTA/TG curves for all samples (A, C and D) and their thermal behavior is similar to those of the TBT. The common feature of all DTA curves is the appearance of an endothermic effect about 100–110 °C which is attributed to the evaporation of organic solvent and desorption of physically adsorbed water. This peak is accompanied by a weight loss which varies depending on composition (~7% for sample A, ~23% – sample C and ~4% for sample D). The differences in the DTA results concern the exothermic effects that are specific for each composition. The DTA/TG curves for the sample A ($80TiO_2.20TeO_2$) showed two broad exothermic peaks registered at about 235 and 285 °C (Fig. 3a). The first one is related to the beginning of the decomposition of the organic groups (weight loss is ~8%) as in the pure TBT. The second exothermic effect appeared at slightly higher temperature (285 °C) with around 15% weight loss which suggests strong combustion of the organic components [34]. The increasing of the curve intensity about 400 °C suggests the presence of an exothermic effect due to the oxidation of Te to TeO_2. For comparison, other authors established that the oxidation proceeded at similar temperatures [9, 35, 36]. As it can be seen from the DTA/TG curves of sample C ($80TiO_2.20B_2O_3$) two exothermic effects are distinguished (Fig. 3b). The first and sharper one is observed about 310 °C and could be related to the intense combustion of the alkoxide groups bonded to the Ti-atom. According to the TG curve this peak is accompanied by strong weight loss (~ 65%). Contribution to this exothermic effect has also the crystallization of TiO_2 (anatase) established by XRD which is further discussed in the paper. The second exothermic peak (about 570°C) is as-

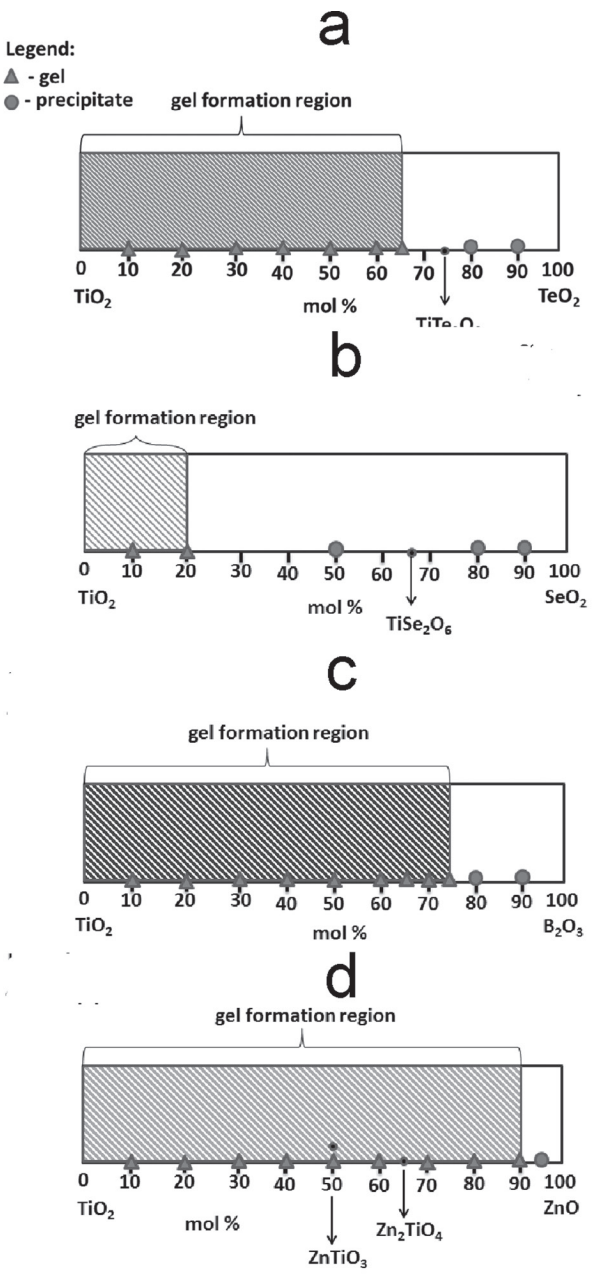

Fig. 2. Gel formation regions in the binary systems: $TiO_2 – TeO_2$ (a), $TiO_2 – SeO_2$ (b), $TiO_2 – B_2O_3$ (c) and $TiO_2 – ZnO$ (d).

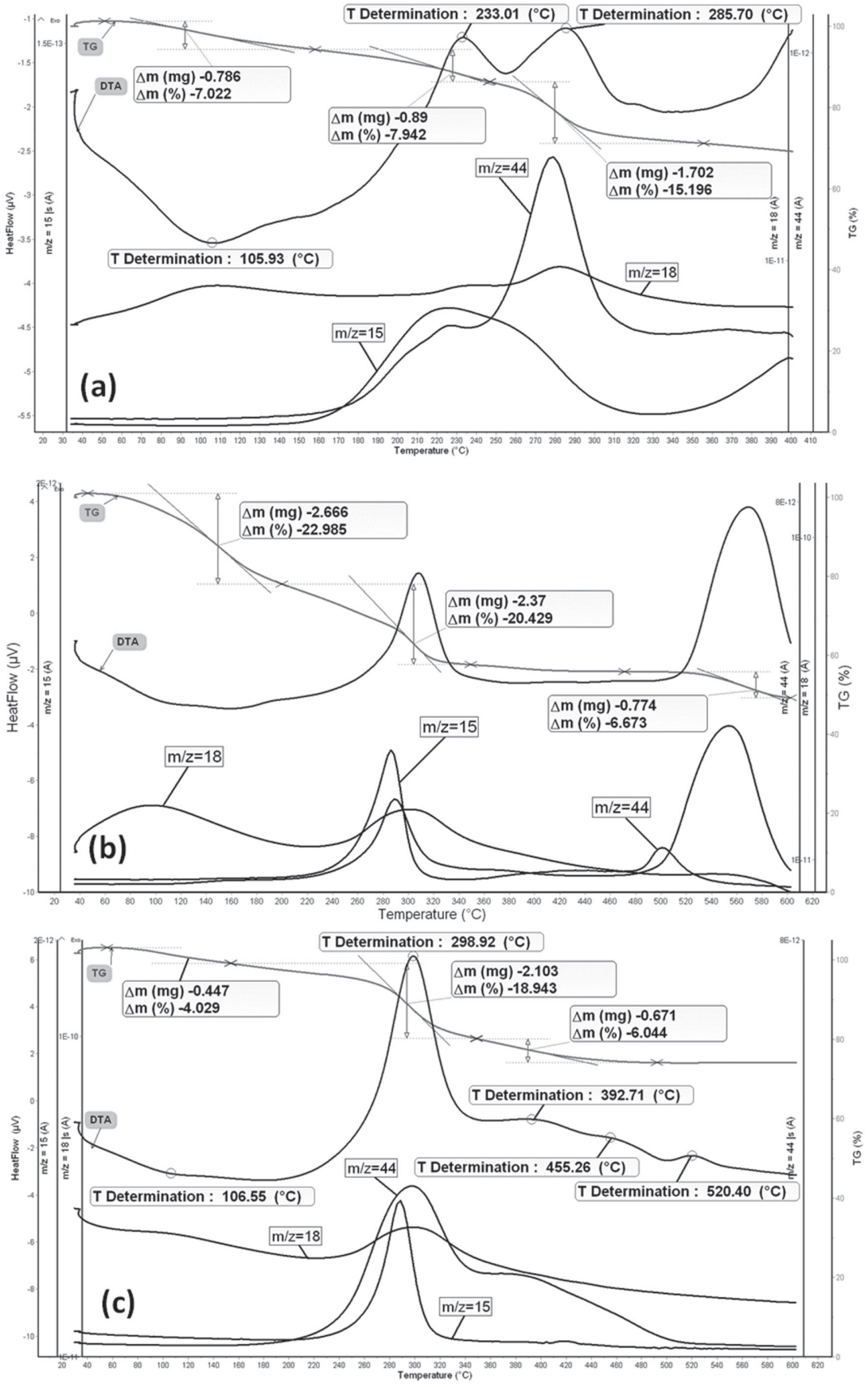

Fig. 3. DTA–TG curves of samples A ($80TiO_2.20TeO_2$) (a), C ($80TiO_2.20B_2O_3$) (b), D ($80TiO_2.20ZnO$) (c).

sociated with the slow oxidation of residual carbon and release of CO_2 accompanied by a little weight loss about 7%. Similar data are obtained by other authors [35–37]. Several exothermic effects at 300, 400, 455 and 520 °C were found in sample D ($80TiO_2.20ZnO$) (Fig. 3c). The first one (~ 300 °C) is the strongest and broadest one and it is related by analogy with the previous samples to the intense combustion of organics (the weight loss is ~ 20%). The next two and small exothermic peaks (at 400 and 455 °C) could be attributed to the crystallization of TiO_2 (anatase) and $ZnTiO_3$ crystalline phases (weight loss about 6%). The last one at 520 °C is associated with the slow oxidation of residual carbon and release of CO_2.

Phase transformations and morphology

The obtained by XRD analysis data are summarized in Table 1. According to the XRD patterns, all samples are amorphous at 200 °C and only in XRD pattern of sample A ($80TiO_2.20TeO_2$) unknown peaks probably due to the organics were detected (Fig. 4). Upon heating, in the temperature range 200–400 °C composite materials consisting of amorphous part and crystalline phases are obtained. For sample A in this temperature range only metallic tellurium (JCPDS 78-2312) was detected, while in the other three samples the first crystals of TiO_2 (anatase) (JCPDS 78-2486) appeared (Fig. 4). It is worth noting that the anatase appeared earlier (300 °C) in samples B ($80TiO_2.20SeO_2$) and C ($80TiO_2.20B_2O_3$) than in sample D ($80TiO_2.20ZnO$), where it was barely registered at 400 °C. For comparison, in pure TBT gel, the anatase crystallization occurs at 400 °C [32]. Irrespective of the fact that inorganic precursors (H_6TeO_6, H_2SeO_3 and H_3BO_3) were used, we found similar results for phase transformations obtained by other authors [7, 8, 34, 38–40]. The average crystallites size of metallic Te (in sample A) is 27 nm at 250 °C and it increased up to 42 nm at higher temperatures (300 and 400 °C). Tellurium is fully oxidized to TeO_2 (JCPDS 42-1365) above 400 °C in sample A. In addition to TeO_2 the heating at 500 °C of this sample showed presence of $TiTe_3O_8$ (JCPDS 50-0250) and TiO_2 (anatase). At this temperature only TiO_2 (anatase) is registered in the XRD patterns of samples B and C, while in sample D – TiO_2 (anatase) with $ZnTiO_3$ (cubic, JCPDS 39-0190) crystalline phases. At further heating (600 °C), partial transformation of anatase to rutile (JCPDS 21-1276) is detected only in sample B ($80TiO_2.20SeO_2$) while rutile appeared in the other samples at 700°C. The average crystallite size of anatase in all samples (A, B, C and D) heated in the temperature range 400–600 °C was summarized in Table 2. As it is seen from the Table, at 500 °C sample A ($80TiO_2.20TeO_2$) and B ($80TiO_2.20SeO_2$) exhibited more nanosized crystallites (sample A – 10 nm, sample B – 12 nm) in comparison to samples C ($80TiO_2.20B_2O_3$, 75 nm) and D ($80TiO_2.20ZnO$, 90 nm). At higher temperature (600 °C) this tendency is preserved.

Sample B ($80TiO_2.20SeO_2$) heat treated at 200 and 400 °C was subjected for SEM (Fig. 5) and TEM (Fig. 6) investigations in order to verify its morphology as well as the existence of selenium. As one can see, small pieces as a result from the crashing of the monolithic gels during the drying process are observed with average size about 50–150 μm. Small bright spots are distinguished in some areas on the sample surface. The microprobe

Table 1. Detected by XRD crystalline phases in the investigated compositions

Compositions	Detected crystalline phases by XRD					
	200 °C	300 °C	400 °C	500 °C	600 °C	700 °C
$80TiO_2.20TeO_2$	metal-organic compounds	amorphous + Te	amorphous + Te	anatase + α-TeO_2 + $TiTe_3O_8$	anatase + $TiTe_3O_8$	anatase + rutile + $TiTe_3O_8$
$80TiO_2.20SeO_2$	amorphous	amorphous + anatase	anatase	anatase	anatase + rutile	rutile + anatase
$80TiO_2.20B_2O_3$	amorphous	amorphous + anatase	anatase	anatase	anatase	anatase
$80TiO_2.20ZnO$	amorphous	amorphous	anatase	anatase + $ZnTiO_3$	anatase + $ZnTiO_3$	anatase + rutile + $ZnTiO_3$

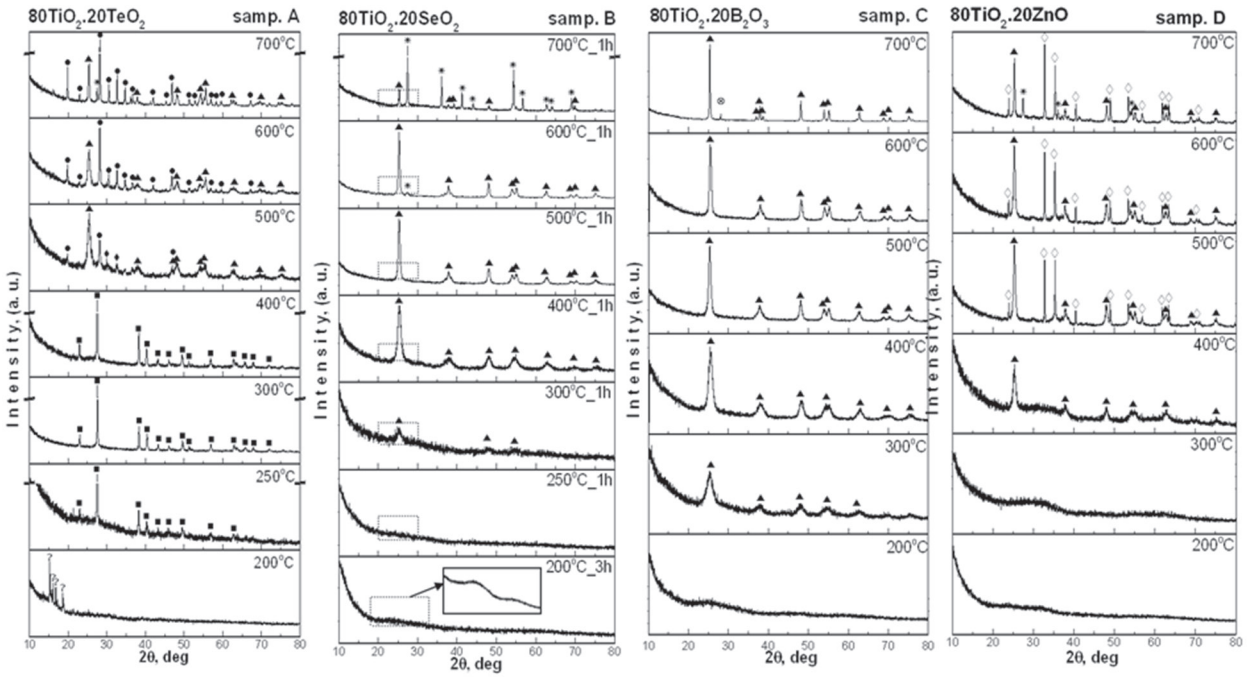

Fig. 4. XRD patterns of the: (a) investigated samples A, B, C and D; (b) pure Ti butoxide (TBT), (■) Te, (♦) α-TeO_2, (▲) TiO_2-anatase, (✳) TiO_2-rutile, (●) $TiTe_3O_8$, (⊙) H_3BO_3, (◊) $ZnTiO_3$ (cubic).

Table 2. Average crystallite size of anatase in all samples (A, B, C and D)

TiO_2 (anatase) crystallite size (nm)										
Sample A $80TiO_2.20TeO_2$		Sample B $80TiO_2.20SeO_2$			Sample C $80TiO_2.20B_2O_3$			Sample D $80TiO_2.20ZnO$		
500 °C	600 °C	400 °C	500 °C	600 °C	400 °C	500 °C	600 °C	400 °C	500 °C	600 °C
10	50	10	12	47	45	75	82	45	90	95

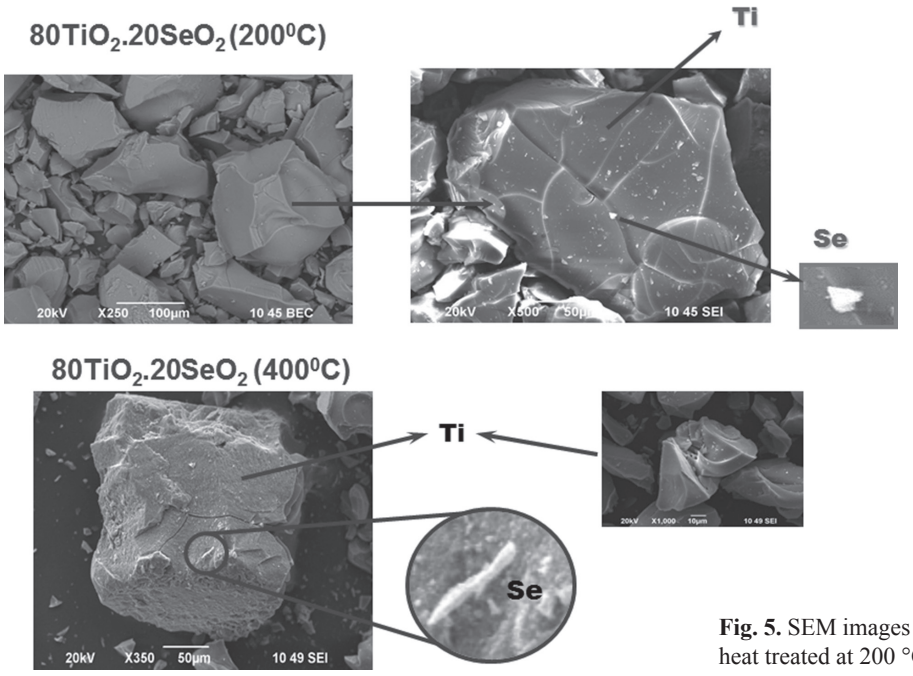

Fig. 5. SEM images of composition B ($80TiO_2.20SeO_2$) heat treated at 200 °C (a) and 400 °C.

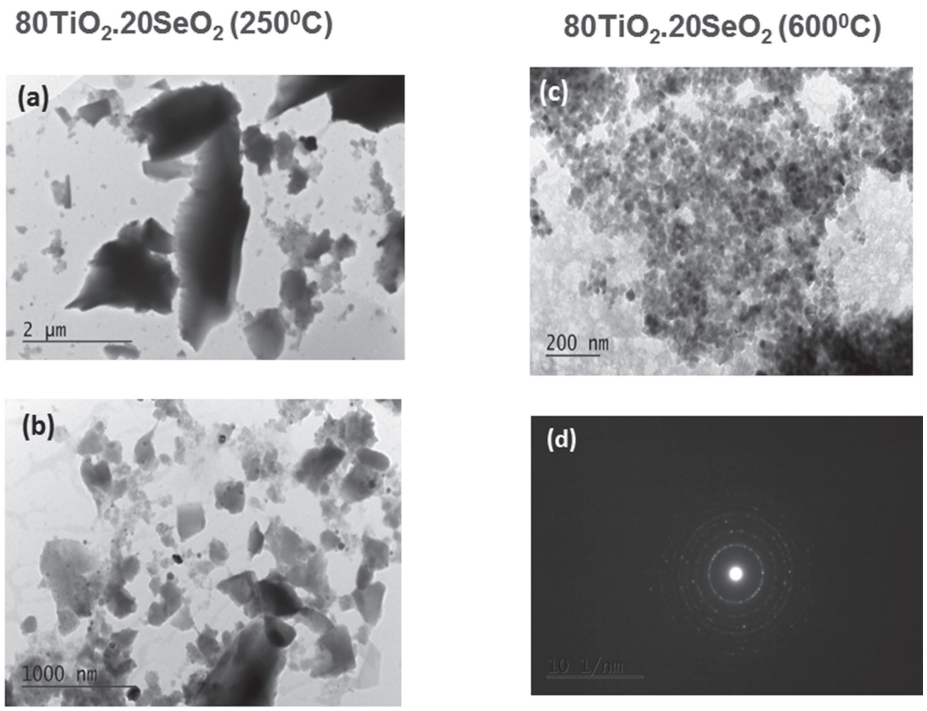

Fig. 6. Bright field TEM images of sample B ($80TiO_2.20SeO_2$) heat treated at 250 °C (a, b) and 600 °C (c); selected area electron diffraction image (SAED) pattern from sample B heat treated at 600 °C (d).

analysis showed that selenium is segregated in these parts which mean that it is not evaporated even at 400 °C (Table 3).

The TEM observations of sample B heat treated at 200 and 600 °C were performed (Fig. 6a–c). At the lower temperature it was confirmed that the sample is amorphous (Fig. 6a, b), while at 600 °C spherical particles were observed with average size of 40 nm (Fig. 6c). The selected area electron diffraction data (SAED) exhibited presence of polycrystalline anatase (Fig. 6d). This result is in good accordance to the XRD data already discussed above.

Analysis of the results

From the above pointed results, it is obvious that two questions 1) related to the amorphous phase in all samples and 2) the stability of anatase crystals at higher temperatures arose. In order to elucidate these problems, a comparison between our results and some published data concerning the stability of the amorphous phase in the investigated TiO_2 – containing systems is made. As it was mentioned above, in our samples the amorphous halo is observed up to 300 °C, and gradually decreases with the increase

Table 3. Microprobe analysis performed in different points of the sample B ($80TiO_2.20SeO_2$) heat treated at 200 and 400 °C

Elements	Microprobe analysis (at%) of sample $80TiO_2.20SeO_2$ (mol%) 27Ti/6Se/67O (at%)	
	200 °C	400 °C
Ti	8.32	27.11
Se	1.76	8.06
O	66.67	64.83
C	23.25	–

of temperature. Applying different method of synthesis and components, many authors [24, 41–48] pointed out different temperatures (from 100 to 400 °C) at which TiO_2 is in amorphous state.

Reznitskij and Filipova [49] found that if the bond energy value of the second component is higher than that of the TiO_2 matrix, this leads to the stabilization of the amorphous matrix and vice versa. Generally, Cr, Al, Zr favor the amorphous state up to ~ 400 °C, while Fe and Cu facilitate the crystallization at about 250 °C. As the Te-O (3.42 eV), Se-O (3.63 eV), B-O (5.55 eV) and Zn-O (2.94 eV) bond energies are higher than that of Ti-O (1.45 eV), the amorphous state in our samples is preserved up to ~300 °C.

The second question is related to the stability of the anatase phase at higher temperature. The type of second and third component and the particle size dimensions may be responsible for the transformation anatase to rutile. According to Hanaor and Sorrell [50] the small cations of low valence (< 4) should promote the anatase to rutile transformation while the large cations of high valence (> 4) should inhibit it. Having in mind these suggestions it is expected B and Zn to be promoters while Te and Se to inhibit, but our results did not confirmed this statement. Generally, the kinetics of the anatase to rutile transformation is affected strongly by many factors and the understanding of this problem is still not exhausted [51, 52].

CONCLUSIONS

The gel formation regions in the binary $TiO_2 – M_nO_m$ ($M_nO_m = TeO_2, SeO_2, B_2O_3, ZnO$) systems were determined. By the new combination of organic and inorganic precursors a simple route for obtaining of homogeneous gels is offered. It was established that the addition of H_2SeO_3 or H_3BO_3 to Ti butoxide stimulates the earlier TiO_2 (anatase) crystallization (~ 300 °C) while in presence of Zn acetate or H_6TeO_6 the anatase appears at higher temperatures 400 and 500 °C, respectively. No formation of binary crystalline compounds is detected during the heating in the TiO_2–SeO_2 and TiO_2–B_2O_3 systems while in the TiO_2–ZnO and TiO_2–TeO_2 ones, $ZnTiO_3$ and $TiTe_3O_8$ respectively, were found. Nanocomposites consisting of amorphous phase along with metallic Te or TiO_2 (anatase) are derived from gels up to 300 °C while above 400 °C oxide crystalline phases (anatase, α-TeO_2, $TiTe_3O_8$, $ZnTiO_3$ and rutile) only were observed.

Acknowledgements: *The authors are grateful to the financial support of The Ministry of Education and Science of Bulgaria, Contract No ДНТС/India 01/6, 2013: Bulgarian-Indian Inter-governmental Programme of Cooperation in Science and Technology.*

REFERENCES

1. S. Sakka, Handbook of sol-gel science and technology: processing, characterization and applications, vols. I, II and III, Kluwer Academic Publishers, The Netherlands, 2004
2. A. Bachvarova-Nedelcheva, R. Iordanova, K. L. Kostov et al., *Opt. Mater.*, **34**, 1781 (2012).
3. M. Udovic, P. Thomas, A. Mirgorodsky, O. Durand, M. Soulis, O. Masson, T. Merle-Méjean, J.C. Champarnaud-Mesjard, *J. Sol. St. Chem.*, **179**, 3252 (2006).
4. E. R. Barney, A. C. Hannon, D. Holland, N. Umesaki, M. Tatsumisago, R. G. Orman & S. Feller, *J. Phys. Chem. Let.*, **4**, 2312 (2013).
5. J.-C. Sabadel, P. Armand, P. E. Lippens, D. C. Herreillat & E. Philippot, *J. Non-Cryst. Sol.*, **244**, 143 (1999).
6. L. Weng, S. Hodgson, *Mater. Sci. Engineer. B*, **87**, 77 (2001).
7. T. Hayakawa, H. Koyama, M. Nogami, et al., *J. Univ. Chem. Technol. Metall.*, **47** (4), 381 (2012).
8. L. Weng, S. Hodgson, X. Bao, K. Sagoe-Crentsil, *Mater. Sci. Engineer. B*, **107**, 89 (2004).
9. L. Weng, S. Hodgson, *J. Mater. Sci.*, **36**, 4955 (2001).
10. S. Hodgson, L. Weng, *J. Mater. Sci.*, **37**, 3059 (2002).
11. T.T.Y. Tan, C. K. Yip, D. Beydoun, R. Amal, *J. Chem. Eng.*, **95**, 179 (2003).
12. P. Zhang, D. L. Sparks, *Environm. Sci. Technol.*, **24**, 1848 (1990).
13. S. Sanuki, T. Kojima, K. Arai, S. Nagaoka, H. Majima, *Metall. Mater. Trans. B*, **30**, 15 (1999).
14. S. – Y. Zhang, X. Chen, Y. Tian, B.K. Jin, J.X. Yang, *J. Crystal Growth*, **304**, 42 (2007).
15. V. Stengl, S. Bakardjieva, J. Bludska, *J. Mater. Sci.*, **46**, 3523 (2011).
16. V. Nguyen, R. Amal, D. Beydoun, *J. Photochem. Photobiol. A: Chemistry*, **179**, 57 (2006).
17. A. Irwin, J. Holmgren & J. Jonas, *J. Non-Cryst. Solids*, **101**, 249 (1988).
18. K. Jung, S. Park & S. Ihm, *Appl. Catal. B: Environmental*, **51**, 239 (2004).
19. A. Fujishima, T. N. Rao, D. A. Tryk, *J. Photochem. Photobiol. C: Photochem. Rev*, **1**, 1 (2000).
20. C. Hariharan, *Appl. Catal. A: Gen.*, **304**, 55 (2006).
21. G. Marcì, V. Augugliaro, M. J. López-Muñoz, C. Martín, L. Palmisano, V. Rives, M. Schiavello, R. J. D. Tilley, A.-M. Venezia, *J. Phys. Chem. B*, **105**, 1026 (2001).
22. X. Xu, J. Wang, J. Tian, X. Wang, J. Dai, X. Liu, *Ceram. Intern.*, **37**, 2201 (2011).
23. C. Shifu, Z. Wei, L. Wei, Z. Sujuan, *Appl. Surf. Sci.*, **255**, 2478 (2008).

24. R. Iordanova, R. Gegova, A. Bachvarova-Nedelcheva, Y. Dimitriev, *Phys. Chem. Glasses: Eur. J. Glass Sci. Technol. B*, **56** (4), 128 (2015).
25. R. Gegova, A. Bachvarova-Nedelcheva, R. Iordanova, Y. Dimitriev, *Bulg. Chem. Commun.*, **47** (1), 378 (2015).
26. R. Gegova, R. Iordanova, A. Bachvarova-Nedelcheva, Y. Dimitriev, *J. Chem. Technol. Metall.*, **50** (4), 449 (2015).
27. A. Bachvarova-Nedelcheva, R. Gegova, A. Stoyanova, R. Iordanova, V. E. Copcia, N. Ivanova, I. Sandu, *Bulg. Chem. Commun.,* **46** (3), 585 (2014).
28. A. Bachvarova-Nedelcheva, R. Iordanova, A. Stoyanova, R. Gegova, Y. Dimitriev, A. Loukanov, *Centr. Eur. J. Chem.*, **11** (3), 364 (2013).
29. R. Iordanova, A. Bachvarova-Nedelcheva, R. Gegova and Y. Dimitriev, *Bulg. Chem. Commun.*, **45** (4), 485 (2013).
30. A. Bachvarova-Nedelcheva, R. Gegova, R. Iordanova, A. Stoyanova, Y. Dimitriev and N. Ivanova, *Nanoscience and Nanotechnology*, **13,** 56 (2013).
31. S. Doeuff, M. Henry, C. Sanchez, J. Livage, *J. Non-Cryst. Sol.*, **89**, 206 (1987).
32. R. Iordanova, A. Bachvarova-Nedelcheva, R. Gegova, Y. Dimitriev, *J. Sol-Gel Sci. Technol.*, **79** (1), 12 (2016).
33. S. N. B. Hodgson, L. Weng, *J. Non-Cryst. Sol.*, **276**, 195 (2000).
34. A. Lecomte, F. Bamiere, S. Coste et al., J. Europ. Cer. Soc. **27**, 1151 (2007).
35. F. Saylikan, M. Asilturk, H. Saylikan, Y. Onal, M. Akarsu, E. Aprac, *Turk. J. Chem.*, **29**, 697 (2005).
36. J. Madarasz, A. Braileanu, M. Crisan, G. Pokol, *J. Anal. Appl. Pyrol.*, **85**, 549 (2009).
37. C. J. Brinker & G. Scherer, "*Sol-gel science: the physics and chemistry of sol-gel processing*", Academic Press Inc, San Diego, CA, 1990.
38. S. Coste, A. Lecomte, P. Thomas, T. Merle-Mejean, J. C. Champarnaud-Mesjard, *J. Sol-Gel Sci. Techn.*, **41**, 79 (2007).
39. S. Hodgson, L. Weng, *J. Non-Cryst. Sol.*, **297**, 18 (2006).
40. H.-Y. Wei, W.-H. Huang, Z.-B. Feng, D.-W. Li, *Mater. Sci. Engineer. B*, **164**, 51 (2009).
41. Z. Zhang, P. Maggard, *J. Photochem. Photobiol. A:Chem*, **186**, 8 (2007).
42. M. J. Alam, D. C. Cameron, *J. Sol-Gel Sci. Technol.*, **25**, 137 (2002).
43. D. Svadlak, J. Shanelova, J. Malek, L. Perez-Maqueda, J. Criado, T. Mitsuhashi, *Thermochim. Acta*, **414**, 137 (2004).
44. Ch.-W. Hsieh, A.S.T. Chiang, C.C. Lee & Sh.-J. Yang, *J. Non-Cryst. Sol.*, **144**, 53 (1992).
45. M. Khanna, S. Wongnawa, *Mater. Chem. Phys.*, **110**, 166 (2008).
46. H. Li, G. Shao, Z. Chen, B. Song, G. Han, *J. Am. Ceram. Soc.*, **93** (2), 445 (2010).
47. A. Shalaby, Y. Dimitriev, R. Iordanova, A. Bachvarova-Nedelcheva and Tz. Iliev, *J. Univ. Chem. Techn. Metall.*, **46** (2), 137 (2011).
48. A. Shalaby, A. Bachvarova-Nedelcheva, R. Iordanova, Y. Dimitriev, *J. Chem. Techn. Metall.*, **48** (6), 585 (2013).
49. L. A. Reznickij, S. E. Filipova, *Vestnik Moskovskovo Universiteta*, ser. 2, Chemistry, **38** (2), 132, (1997) (in Russian).
50. D. A. H. Hanaor, Ch. C. Sorrell., *J. Mater. Sci.*, **46**, 855 (2011).
51. H. Zhang, J. Banfield, *J. Phys. Chem.* B, **104**, 3481 (2000).
52. H. Zhang, J. Banfield, *J. Mater. Chem.*, **8** (9), 2073 (1998).

КРИСТАЛИЗАЦИЯ НА ГЕЛИ В БИНАРНИТЕ СИСТЕМИ $TiO_2–M_nO_m$ ($M_nO_m = TeO_2, SeO_2, B_2O_3, ZnO$)

А. Д. Бъчварова-Неделчева[1]*, Р. С. Йорданова[1], Р. Д. Гегова[1], Я. Б. Димитриев[2]

[1] *Институт по Обща и Неорганична Химия, БАН, ул. „Акад. Г. Бончев“, бл. 11, София 1113, България*
[2] *Химикотехнологичен и Металургичен Университет, бул. „Кл. Охридски“, 1756 София, България*

Постъпила октомври, 2016 г.; приета декември, 2016 г.

(Резюме)

Настоящото изследване е посветено на зол-гелния синтез и фазово характеризиране на двукомпонентни прахове $TiO_2 – M_nO_m$ ($M_nO_m = TeO_2, SeO_2, B_2O_3, ZnO$) с номинален изходен състав $80TiO_2.20M_nO_m$. Проверено е влиянието на различни компоненти върху фазообразуването в посочените състави. Според рентгенофазовия анализ, нагретите до 300 °C гели показват преобладаващо аморфна фаза и формиране на метален телур или TiO_2 (анатаз). Количеството на аморфната фаза постепенно намалява с увеличаване на температурата но все още се забелязва при 500 °C. По-нататъшното увеличаване на температурата (700 °C) води до получаването на полифазен продукт, съдържащ едновременно няколко кристални фази (TiO_2 – рутил, анатаз, $TiTe_3O_8$ и $ZnTiO_3$). Установено бе, че добавянето на H_2SeO_3 и H_3BO_3 стимулира по-ранната кристализация на TiO_2 (анатаз) около 300 °C, докато в присъствие на цинков ацетат или телурова киселина тази фаза се появява съответно при около 400, 500 °C. За сравнение, при нагряване на чист титанов бутоксид, анатазът кристализира около 400 °C.